Study of fringing-field effects on the capacitance of a dielectric disk with a circular conducting hole

Jian-Zhong Bao and Christopher C. Davis
Department of Electrical Engineering, University of Maryland, College Park, Maryland 20742
(Received 23 December 1992)

The capacitance of a thin dielectric sheet with a conducting hole is strongly influenced by the fringe effects around the edges of the hole, particularly when the hole size beomes comparable to the size of the sheet. We present here a numerical study of this situation. By a finite-difference scheme, the potential, field, and surface-charge densities in and around the hole are calculated. The sharp edge of the hole represents a singularity, and the asymptotic behavior of the field and surface-charge densities in the vicinity of the singular point are discussed both analytically and numerically. It is found that the scaled difference between a numerical simulation and the simple parallel-plate-capacitor formula changes with the relative size of the hole in a composite power-law relation.

PACS number(s): 41.20.Cv

I. INTRODUCTION

There are many practical situations in which a knowledge of the correction to the formula for simple parallel-plate capacitance because of the nonuniform charge distribution near edges or holes is needed. The simple formula for parallel-plate capacitance is

$$C=\epsilon_0\epsilon_d\frac{S}{d}\ , \tag{1}$$

where ϵ_d is the relative dielectric constant of the medium between the plates, ϵ_0 is the permittivity of the vacuum, S is the area of the plates, and d is the distance between them. In general, when $\sqrt{S}\gg d$, the correction due to the fringe field can be neglected. However, when this condition is not satisfied, or when the correction has to be taken into account even when it is small, then it becomes interesting to calculate the correction to Eq. (1) due to the fringing field near an edge. There have been some approximate treatments that take the nonuniform distribution of charge near the edge into account, but they provide only a first-order correction [1]. An alternative approach involves finding the potential and charge distribution by solving the appropriate boundary problem. Different boundary geometries will lead to different configurations of the fringing field, and except in a few cases there is no simple or even possible analytical solution, and therefore the numerical methods must be used. The boundary problem we have encountered is that involving a circular dielectric disk with a circular hole at its center embedded in a conducting medium, where the hole is the only current pathway between the upper and the lower regions, as shown in Fig. 1. There are several potential applications where this geometry occurs. In biology, filters made from polymeric or ceramic materials that have many small holes are used for species separation, and for embedding cells and dielectric particles. In electrolyte-solution systems the field distribution in and around the hole is of interest. Small holes can also be used for controlled effusion of neutral and charged species in both liquid and gaseous media. Usually it is very difficult or impossible to solve analytically boundary problems that involve some kind of discontinuity in geometry, such as edges and corners, or in dielectric properties of media as in inhomogeneous systems. Although the conformal-mapping method is helpful in solving for the fringing field in some simple two-dimensional (2D) boundary problems by transforming the boundary to a soluble form, unfortunately, this is only applicable in a limited number of cases [2].

Electrically, a dielectric disk can be modeled as a capacitor, which is perfectly described by Eq. (1) if there are no holes in the disk. However, when there is a hole at its center, the disk, including the conducting hole, has to be modeled as a capacitor in parallel with a resistor. The hole will affect the potential and charge distribution around it, and the difference between the true value of the capacitor and Eq. (1) increases as the relative size of the hole increases. In what follows we will determine the effect on the capacitance of a finite disk caused by a small

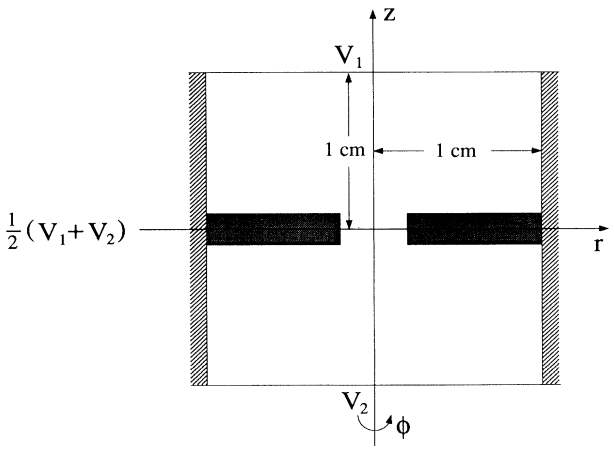

FIG. 1. A schematic diagram of the geometry studied. A dielectric disk is embedded in a conducting cylinder, and a hole in the disk is the only current pathway between the upper and lower conducting regions.

hole at its center. We neglect fringing fields at the outer edge of the disk as, in practice, we view the disk as a circular region that is contiguous with an effectively infinite dielectric slab. Our final result will, therefore, allow us to determine the capacitance per unit area of a large dielectric slab, through which there are many identical circular holes. The separation of the individual holes is assumed to be large enough so that each provides an independent fringing-field correction to the capacitance.

In this study we will determine the distribution of potential, field, and surface-charge densities along the interface between the dielectric and conducting medium, and finally evaluate a correction to the ideal capacitance of the disk. Because a regular boundary geometry is involved, the finite-difference (FD) method is very suitable. The FD method is an extremely useful tool for solving partial differential equations and has been intensively used in many areas of science and engineering because it is both simple to implement and reliable. In this paper we present a FD scheme to solve this specific boundary problem on a uniform mesh. The effect of the singularity at the hole edge is also discussed. Adjustment of the size of the hole shows that the relative difference between the capacitance calculated numerically and that determined from Eq. (1) changes with the ratio of hole area to total area in a composite power-law relation.

II. THE BOUNDARY PROBLEM

This inhomogeneous system consists of two homogeneous regions: a conducting medium and a dielectric disk. It is well known that in order to determine the potential distribution of a steady current distribution in an inhomogeneous region, where there are no sources and sinks, it is necessary to solve the current continuity equation,

$$\nabla\cdot(\sigma\nabla\phi)=0 , \tag{2}$$

where ϕ is the potential function, and σ is the conductivity. In each of the homogeneous media, Eq. (2) can be replaced by the Laplace equation $\nabla^2\phi=0$. Because of the symmetry about the center plane and z axis of the system, we only need to deal with the first quadrant. We also confine our discussion to a unit domain with 1 cm length in both r and z directions as shown in Fig. 1, and assume $V_1 > V_2$. For the sake of simplicity, and without loss of generality, ϕ is scaled into a dimensionless form ψ by the following relation:

$$\psi=2\left[\frac{\phi-V_2}{V_1-V_2}\right]-1 . \tag{3}$$

Because the capacitance is determined from an integration of the ratio of the surface-charge density to the associated potential values on the surface of the dielectric, this transformation will not affect the result for the capacitance. There is no current passing across the boundaries at $r=1$ cm and 0, and it is also reasonable to assume that the field is in the z direction at $r=1$ cm in the dielectric since we are only interested in the fringing field around the hole. With the above conditions, we have the following governing equation for the scaled potential function ψ in the cylindrical coordinate system:

$$\frac{\partial^2\psi}{\partial r^2}+\frac{1}{r}\frac{\partial\psi}{\partial r}+\frac{\partial^2\psi}{\partial z^2}=0, \quad 0\le r,\ z\le 1 , \tag{4}$$

$$\psi|_{z=1}=1, \quad \psi|_{z=0}=0, \quad \frac{\partial\psi}{\partial r}|_{r=0}=0, \quad \frac{\partial\psi}{\partial r}|_{r=1}=0 , \tag{5}$$

which is a two-dimensional elliptic equation with combined Dirichlet and Neumann boundary conditions. Usually, when a function is cast in a dimensionless form, all unnecessary symbols and units are removed and the problem appears in a very general and simple form. Besides the continuity of the potential function, the boundary conditions at the interface between the conducting medium and dielectric disk are

$$\begin{aligned}&\sigma_c\left[\frac{\partial\psi}{\partial n}\right]_c-\sigma_d\left[\frac{\partial\psi}{\partial n}\right]_d=0 ,\\ &\epsilon_c\left[\frac{\partial\psi}{\partial n}\right]_c-\epsilon_d\left[\frac{\partial\psi}{\partial n}\right]_d=-\frac{\rho_s}{\epsilon_0} ,\end{aligned} \tag{6}$$

where subscript c and d denote conducting medium and dielectric, respectively; ρ_s is the scaled surface-charge density at the interface, and $\mathbf{n}$ is a unit vector with a direction defined normal to the interface and outwards from the dielectric. Because $\sigma_d=0$ and $\sigma_c\neq 0$ at the interface, we have

$$\left[\frac{\partial\psi}{\partial n}\right]_c=0, \quad \left[\frac{\partial\psi}{\partial n}\right]_d=\frac{\rho_s}{\epsilon_0\epsilon_d} , \tag{7}$$

where the first of these relations is to be used with Eqs. (4) and (5) to solve ψ, and the second one is for finding the surface-charge densities at the interface.

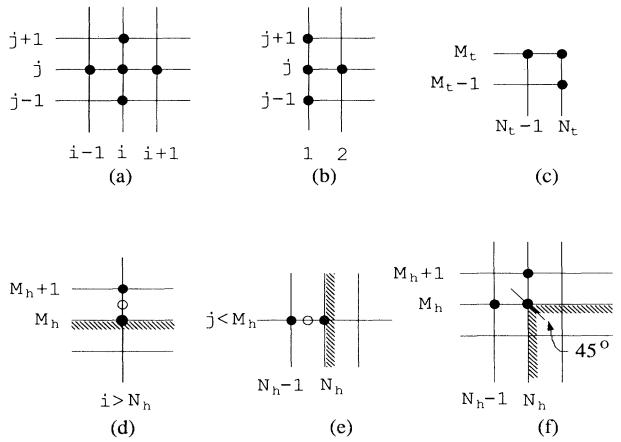

FIG. 2. Schematic diagrams for finite-difference lattice in (r,z) plane: (a) the standard five-point discretization for the nodes not at the interface and the boundary; (b) discretization for the nodes on the z axis but not at the corners; (c) discretization for the corner node (N_t,M_t); (d) discretization for the nodes on the top surface of the disk: the open circle is an imaginary node; (e) discretization for the nodes on the wall of the hole: the open circle is an imaginary node; (f) discretization for the apex node of the edge (N_h,M_h) along the 45° direction.

III. FINITE-DIFFERENCE DISCRETIZATION

The fundamental principle of the FD method for solving differential equations is that derivatives are replaced by difference expressions that use truncated Taylor series. The solution is obtained with the following steps: (i) discretizing the physical region into a finite set of grid nodes; (ii) transforming the governing equation and the boundary conditions into finite-difference forms at each node, which gives a set of linear equations; and (iii) solving these linear equations to get the numerical solutions on the nodes. Different methods of truncation will lead to different forms for the FD operators, which give different orders of approximation for the differential equations. We apply the most common second-order center-difference method, with which there are five points involved in each of the linear equations if the nodes are not at a boundary or at the interface between the different media. Figure 2(a) shows a node and its immediate four neighbors. In this way Eq. (4) can be written as

$$\psi(i,j-1)\left[\frac{1}{(\Delta z)^2}\right]+\psi(i-1,j)\left[\frac{1}{(\Delta r)^2}-\frac{1}{2(i-1)(\Delta r)^2}\right]-\psi(i,j)\left[\frac{2}{(\Delta r)^2}+\frac{2}{(\Delta z)^2}\right]$$
$$+\psi(i+1,j)\left[\frac{1}{(\Delta r)^2}+\frac{1}{2(i-1)(\Delta r)^2}\right]+\psi(i,j+1)\left[\frac{1}{(\Delta z)^2}\right]=0\ , \quad (8)$$

where i and j are the node coordinates, and Δr and Δz are the grid steps in the r and z directions, respectively; Δr and Δz are given by

$$\Delta r=\frac{1}{N_t-1},\quad \Delta z=\frac{1}{M_t+1}\ , \quad (9)$$

where N_t and M_t are the total node numbers in the r and z directions, respectively. We choose nodes $(1,j)$, where $j\neq 1$, and M_t, and (N_t,M_t) as examples to show the discretization of the governing equation combined with the boundary conditions. At $r=0$, the z axis, but not at the corners, four points are involved, as shown in Fig. 2(b),

$$\psi(1,j-1)\left[\frac{1}{(\Delta z)^2}\right]-\psi(1,j)\left[\frac{2}{(\Delta r)^2}+\frac{2}{(\Delta z)^2}\right]$$
$$+\psi(2,j)\left[\frac{2}{(\Delta r)^2}\right]+\psi(1,j+1)\left[\frac{1}{(\Delta z)^2}\right]=0\ . \quad (10)$$

For r and $z=1$, three points are involved, as shown in Fig. 2(c),

$$\psi(N_t,M_t-1)\left[\frac{1}{(\Delta z)^2}\right]+\psi(N_t-1,M_t)\left[\frac{2}{(\Delta r)^2}\right]$$
$$-\psi(N_t,M_t)\left[\frac{2}{(\Delta r)^2}+\frac{2}{(\Delta z)^2}\right]=-\frac{1}{(\Delta z)^2}\ . \quad (11)$$

The range occupied by the dielectric is $i>N_h$ and $j<M_h$. Because the interface nodes between the conducting medium and the dielectric present a singularity in the conductivity derivative, the first equation of Eq. (7), rather than Eq. (2), should be employed for these nodes. Equation (7) shows the discontinuity of $\partial\psi/\partial n$ at the interface, therefore in this situation special treatment is required. There are several methods for dealing with interface nodes between two different media [3,4]. We have developed a very simple method that uses an imaginary node between the interface node and its immediate neighbor node beyond the disk, as shown in Figs. 2(d) and 2(e). It is a good approximation that the normal derivative on the interface in the conducting side can be replaced by the FD equation at this imaginary node. So, finally, for the nodes at the surface of the disk, we have

$$\psi(i,M_h+1)-\psi(1,M_h)=0,\quad i>N_h\ , \quad (12)$$

which is shown in Fig. 2(d). For the nodes on the wall of the hole, shown in Fig. 2(e),

$$\psi(N_h,j)-\psi(N_h-1,j)=0,\quad j<M_h\ . \quad (13)$$

Nevertheless, the normal direction of the apex of the edge (N_h,M_h) is not as well defined as that on the flat surface. Because an infinitely sharp edge does not exist in practice, it is reasonable to assume that the normal direction is along the 45° line of the corner shown in Fig. 2(f). Application of the boundary condition on this edge node gives

$$\frac{\Delta l_2}{\Delta l_1+\Delta l_2}\psi(N_p-1,M_p)-\psi(N_p,M_p)$$
$$+\frac{\Delta l_1}{\Delta l_1+\Delta l_2}\psi(N_p,M_p+1)=0\ , \quad (14)$$

where Δl_1 and Δl_2 are defined as

$$\Delta l_1=\frac{\Delta z}{\sqrt{2}\sin(\pi/4+\beta)},\quad \Delta l_2=\frac{\Delta z}{\sqrt{2}\sin(3\pi/4-\beta)}\ , \quad (15)$$

where $\beta=\tan^{-1}(\Delta z/\Delta r)$. There are only N_t equations associated with boundary condition $\psi|_{z=1}=1$, e.g., Eq. (11), which have a nonzero right side, i.e., $b(i,M_t)=-1/(\Delta z)^2$; for all others $b(i,j)=0$. To summarize: to this point the governing equation and boundary conditions have been expressed in terms of a set of linear equations

IV. MATRIX FORMULATION AND GAUSS-SEIDEL ITERATION

For compactness, $\psi(i,j)$ and $b(i,j)$ are transformed into n-dimensional vectors, ψ_k and b_k, where we denote

the nodes with a single integer, i.e., $k=(j-1)N_t+i$, so that each node is uniquely represented. The linear equations discussed above can then be written in matrix form as $\underline{A}\cdot\Psi=\mathbf{B}$, where $\underline{A}$ is the $n\times n$ coefficient matrix, with $n=N_tM_t$. The structure of the sparse matrix $\underline{A}$ involves three diagonal blocks, a structure often seen in FD methods. Because of the presence of the interface, many of the elements in these three blocks are zero: the number of nonzero elements in the matrix is $n_n=5M_tN_t-2M_t-9N_t+7M_h+3N_h+11$, which is much smaller than $n^2=(N_tM_t)^2$. To save computer storage space, a vector is generally formed that contains all the nonzero elements of the sparse matrix, and two integer vectors that give information of column and row for each entry of the vector. Although several software packages have been developed for solving sparse matrix problems [5], because of the well-defined structure of the matrix $\underline{A}$, we have developed our own software to solve these specific sparse linear equations without using two-index vectors. Usually for large sparse systems, an iterative method is efficient in terms of both computer storage and computational time. An iterative method for solving the $n\times n$ linear system starts with an initial approximation $\Psi^{(0)}$ to the solution Ψ, and generates a sequence of vectors $\Psi^{(1)},\Psi^{(2)},\ldots,\Psi^{(\infty)}$ that converges to Ψ. The Gauss-Seidel method uses the most recently found ψ_j $(j\neq i)$ at each iteration to give a new ψ_i,

$$\psi_i^{(k)}=\left[b_i-\sum_{j=1}^{i-1}a_{ij}\psi_j^{(k)}-\sum_{j=i+1}^{n}a_{ij}\psi_j^{(k-1)}\right]\Big/a_{ii}\ , \tag{16}$$

where ψ_i, a_{ij}, and b_i are coefficients of Ψ, $\underline{A}$, and $\underline{\mathbf{B}}$, respectively, and the superscripts k and $k-1$ denote the iteration number of the solution. The summations on the right-hand side of Eq. (16) will be substantially reduced because of the sparsity of the matrix. In practice it is desirable that the coefficient matrix $\underline{A}$ be diagonally dominant, which ensures that the iterative methods converge [6]. In our case, most of the equations are diagonally dominant except for those involving interface nodes, Eqs. (12) and (13), which are the primary reasons for slow convergence of this problem.

V. RESULTS AND DISCUSSION

Equidistant nodes are taken which give uniformly distributed approximation values over the whole region, and all the calculations are done using a 101×99 grid, which gives $\Delta z=\Delta r=0.1$ mm. Potential distributions have been calculated for 11 different radii of the hole in the disk, from which we choose the 0.5-mm hole as an example to show our results. Figure 3 shows the current and equipotential lines in the whole region, which is consistent with an intuitive physical picture. In the dielectric, the field becomes more uniform when it is away from the apex. The distributions of the current flux in the r and z directions, j_r and j_z, are shown in Figs. 4(a) and 4(b), respectively, where we have assumed $\sigma=1$. There is clearly a singularity at the node (N_h,M_h), where a very sharp peak is found. Figure 4(c) shows the spatial variation of the magnitude of the field E_m, where we also see a

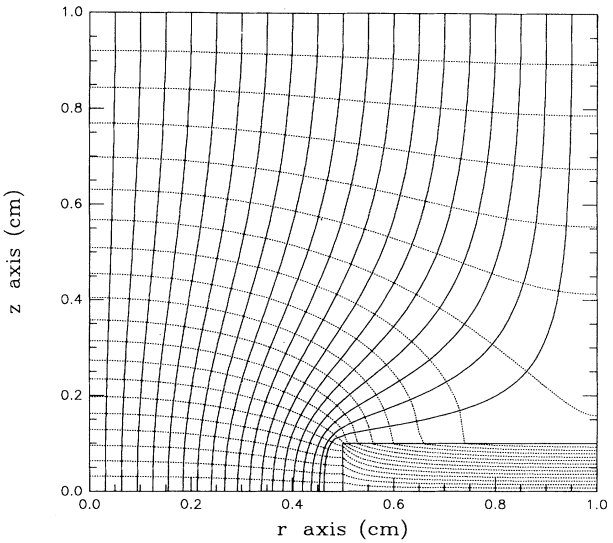

FIG. 3. The equipotential and current lines in the first quadrant for a disk with a 5-mm-radius hole at the center, and a half thickness of 1 mm. The potential difference between any two neighboring equipotential lines is the same.

marked peak at (N_h,M_h): the field inside the dielectric but away from the apex is smoother and stronger. Theoretically, near the apex of the edge the problem can be approximated as a 2D problem, and the potential function in the conducting medium can be written as

$$\psi=\psi(N_p,M_p)+D_1\rho^m\cos(m\theta),\quad 0\le\theta\le\tfrac{3}{2}\pi\ , \tag{17}$$

where ρ is the distance from the apex, and θ is measured from the top surface of the disk. We only take the lowest positive power of ρ into account because ρ is very small. With the boundary conditions at the interface, i.e., $j_\theta=0$ when $\theta=0$ and $3\pi/2$, we have an $m=\frac{2}{3}$. D_1 is a constant and can only be determined from the overall boundary conditions, in which we are not interested. The sign of D_1 can be determined easily: when $\theta=0$, ψ increases while ρ increases, so $D_1>0$. The current flux function can be easily found from $\mathbf{j}=-\sigma\nabla\psi$,

$$j_\rho=-\tfrac{2}{3}D_1\sigma\rho^{-1/3}\cos(\tfrac{2}{3}\theta),\quad j_\theta=\tfrac{2}{3}D_1\sigma\rho^{-1/3}\sin(\tfrac{2}{3}\theta)\ , \tag{18}$$

The potential function in the dielectric in the vicinity of the apex can be written as

$$\psi=\psi(N_p,M_p)+D_2\rho^n\sin(n\theta+D_3),\quad -\frac{\pi}{2}\le\theta\le0\ . \tag{19}$$

With the condition of continuity of the potential function at the interface, we have $n=\frac{2}{3}$, $D_2=2D_1$, and $D_3=\pi/6$, which gives the field function as

$$E_\rho=-\tfrac{4}{3}D_1\rho^{-1/3}\sin\left[\frac{2}{3}\theta+\frac{\pi}{6}\right],\qquad E_\theta=-\tfrac{4}{3}D_1\rho^{-1/3}\cos\left[\frac{2}{3}\theta+\frac{\pi}{6}\right]. \tag{20}$$

Examination of Eqs. (20) and (18) shows that the field strength in the dielectric near the apex is twice that in the conducting medium. The equation for E_θ in Eq. (20), together with Eq. (7), gives the surface-charge densities near the apex,

$$\rho_s|_{\theta=0}=\epsilon_0\epsilon_d\frac{2}{\sqrt{3}}D_1\rho^{-1/3}\ ,$$
$$\rho_s|_{\theta=-\pi/2}=-\epsilon_0\epsilon_d\frac{2}{\sqrt{3}}D_1\rho^{-1/3}\ , \tag{21}$$

which show that the wall of the hole is negatively charged while the top surface of the disk is positively charged. From Eqs. (18) and (21) it is clear that the field strength and surface-charge densities become infinite when ρ approaches zero with a singularity strength of $\frac{1}{3}$. Because of the unbound nature of the potential derivative in this region, the usual FD formulas become inaccurate for some physical parameters, such as energy and current. However, by using a finer mesh around the singular node [7], or using an eigenfunction potential expansion for the nodes near the singularity [8], we can overcome this problem to some extent. These methods may increase the accuracy, but they affect the speed of convergency and make coding more difficult. Although we do not use any special treatment for the singularity, the accuracy of the simulated capacitance will not be affected very much by it because errors introduced around the apex will cancel each other to a large extent because of the opposite signs of the surface charges. The surface-charge densities for the 11 different hole radii are shown in Fig. 5, where for simplicity we let $\epsilon_d=1$. Clearly, the magnitude of the singularity is decreasing while the size of the hole is increasing, which implies that the constant D_1 decreases also. The charge distribution on the top surface of the disk is quite uniform far away from the edge, and the asymptotic limits to the apex are qualitatively consistent with 2D analytical results.

Calculation of the capacitance of the disk can be done without much more effort after finding the potential distribution. The capacitance is obtained from the summation,

$$C_s=\sum_i\frac{\Delta Q_i}{2\psi_i}\ , \tag{22}$$

where i runs along the interface, which includes the top surface and the wall of the hole of the disk, ΔQ_i is a charge element, and ψ_i is the corresponding potential. On the other hand, the capacitance of the disk can be calculated with Eq. (1), where S is only the top surface of the

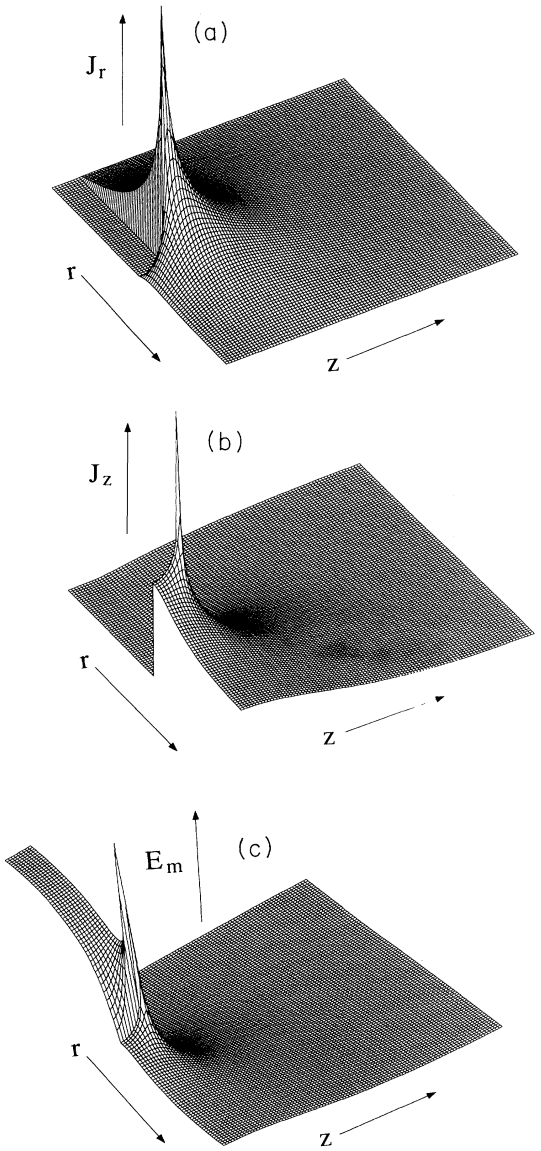

FIG. 4. 3D plots of the distribution of the current flux components (a) j_r, (b) j_z, and (c) the magnitude of the field E_m. Each of these clearly shows a singularity at node (N_h,M_h).

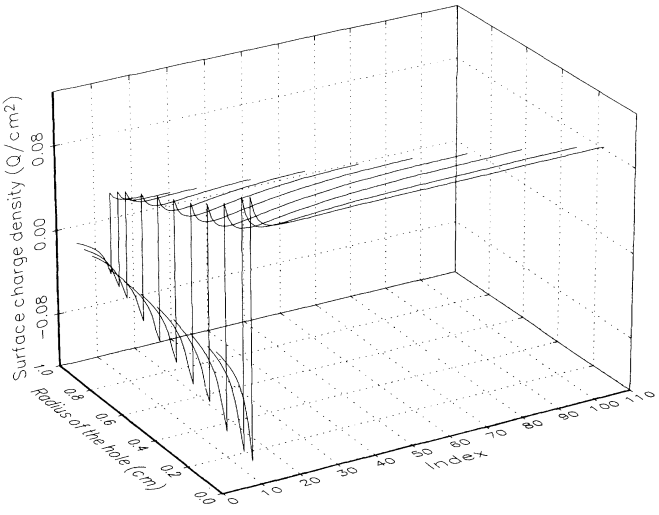

FIG. 5. The charge densities along the interface between the conducting medium and dielectric disk for different relative sizes of hole. The index runs along the interface, and node no. 10 gives the location of the edge. The number of nodes on the surface of the disk is reduced when the size of the hole becomes larger.

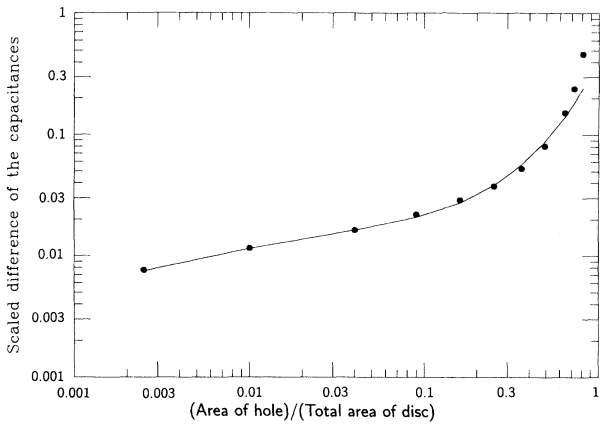

FIG. 6. Nonlinear least-squares fit (solid line) of Eq. (25) to the scaled capacitance difference (●) from FD simulations.

disk. We have found that C is always larger than C_s, which is different from the Kirchhoff's formula [1], where the edge effect causes a larger capacitance. We introduce a scaled function (f_s) and a scaled variable (x),

$$f_s=\frac{C-C_s}{C},\quad x=\frac{S_h}{S_t}\ , \tag{23}$$

to display the effects of the relative hole size on the capacitance, where S_h is the area of hole, and $S_t=S+S_h$ is the total area of the disk including the hole, so x is in the range (0,1). Figure 6 is a plot of $\log_{10}(f_s)$ vs $\log_{10}(x)$, from which it is evident that the curve shows a straight-line section when $x<0.3$, which implies a power-law relation between f_s and x. Calculation of C_s is quite accurate when the size of the hole is small, but less accurate when the size becomes larger because the number of nodes on the surface becomes less. The asymptotic behavior of f_s is important for testing our mathematical model, and can be easily found from the plot,

$$\lim_{x\to 0} f_s=0,\quad \lim_{x\to 1} f_s=1\ . \tag{24}$$

When $x=0$, there is no hole and $C=C_s$; when $x=1$, there is no disk at all, and we assume that C_s approaches zero faster than C. To fit the numerical calculation of f_s, we propose a simple mathematical model with Eq. (24) in mind,

$$f_m=p_1[1-(1-x)^{p_2}-x^{p_3}]+x^{p_4},\quad 0<x<1\ , \tag{25}$$

where $p_1,\ldots,p_4$ are the parameters to be fitted, and are dimensionless since f_s and x are dimensionless. The power-law relation of Eq. (25) is based solely on curve fitting, and implies no specific physics. A criterion for determination of a mathematical model is that the model requiring the smallest number of parameters is preferred without sacrificing the quality of the fit. It is apparent that the coefficient p_1 and exponent p_2 are mainly determined by the straight-line section, which is fairly accurate, while the exponents p_3 and p_4 mostly describe the rest of the curve. Equation (25) has been fitted to the simulated data (f_s) by a nonlinear least-squares (NLS) fit using the Levenberg-Marquardt algorithm [9]. The fitted result is displayed in Fig. 6, where the relatively large deviations between f_m and f_s for points near $x=1$ may result from the relatively large computational errors at these points. The parameters found from the fit are shown in Table I, where all the exponents are less than one.

TABLE I. Parameters found from a NLS fit of Eq. (25) to the data shown in Fig. 6.

$p_1=1.19\pm0.07$	$p_2=0.25\pm0.04$
$p_3=0.61\pm0.04$	$p_4=0.55\pm0.03$

To illustrate these results in a practical way, consider a polycarbonate filter of thickness 10 μm and dielectric constant 3.2 having 10^6 holes of diameter 4 μm/cm^2. The capacitance of the system is about 196 pF/cm^2 when calculated from Eq. (25) where as from the simple capacitance formula, Eq. (1), it is about 248 pF/cm^2, which gives an error of about 25%.

Many types of systems display various parametric power-law relations [10–12], which have been the subject of some attention. The underlying physics of such power-law behavior is still mostly unknown; however, increasing numbers of these phenomena suggest a degree of "universal behavior." Mathematical models are often utilized to describe the physical systems, and devising models is a well-recognized technique, and has been widely used in data analysis. Although models which are merely on the mathematical arguments are often under criticism, they hold the potential to yield the new physics. The power-law dependence we have reported here reflects the power-law behavior of the field near the edge to some extent.

In summary, we have calculated the capacitance of a dielectric disk with a conducting circular hole at the center by a FD scheme. This method provides a simple treatment for the interface between two dissimilar media and the singularity at the apex of the edge of the hole. Analytical and numerical results are consistent in the vicinity of the singularity. The scaled difference in capacitance between the results of the FD method and from the simple parallel-plate-capacitance formula changes with the relative size of the hole in a composite power-law relation.

ACKNOWLEDGMENT

The authors thank the San Diego Supercomputer Center for providing computer time.

[1] L. D. Landau, E. M. Lifshitz, and L. P. Pilaevskii, *Electrodynamics of Continuous Media,* 2nd ed. (Pergamon, New York, 1984).

[2] W. R. Smythe, *Static and Dynamic Electricity,* 3rd ed. (McGraw-Hill, New York, 1965).

[3] F. J. Asencor and M. Panizo, J. Comput. Phys. **95**, 387 (1991).

[4] J. A. Weiss and T. G. Bryant, IEEE Trans. Microwave

Theory Tech. **18**, 595 (1970).

[5] U. Schendel, *Sparse Matrices: Numerical Aspects with Applications for Scientists and Engineers* (Ellis Horwood, West Sussex, UK, 1989).

[6] A. R. Mitchell and D. F. Griffiths, *The Finite Difference Method in Partial Differential Equations* (Wiley, New York, 1980).

[7] I. S. Kim and W. R. Hoefer, IEEE Trans. Microwave Theory Tech. **38**, 812 (1990).

[8] D. H. Sinnott, G. K. Cambrell, C. T. Carson, and H. E. Green, IEEE Trans. Microwave Theory Tech. **17**, 464 (1969).

[9] W. H. Press, B. P. Flannery, S. A. Teukolsky, and W. T. Vetterling, *Numerical Recipes in C* (Cambridge University Press, Cambridge, England, 1988).

[10] J.-Z. Bao, C. C. Davis, and R. E. Schmukler, Biophys. J. **61**, 1427 (1992).

[11] K. L. Ngai, in *Non-Debye Relaxation in Condensed Matter,* edited by T. V. Ramakrishnan and M. R. Lakshmi (World Scientific, New Jersey, 1987).

[12] M. Schroeder, *Fractals, Chaos, Power Laws* (Freeman, New York, 1991).